

Incoherent digital holographic spectral imaging with high accuracy of image pixel registration

Feng-Ying Ma(马凤英), Xi Wang(王茜), Yuan-Zhuang Bu(卜远壮), Yong-Zhi Tian(田勇志), Yanli Du(杜艳丽), Qiao-Xia Gong(弓巧侠), Ceyun Zhuang(庄策云), Jinhai Li(李金海), and Lei Li(李磊)

Citation: Chin. Phys. B, 2021, 30 (**4**): 044202. DOI: 10.1088/1674-1056/abd2aa
Journal homepage: http://cpb.iphy.ac.cn; http://iopscience.iop.org/cpb

What follows is a list of articles you may be interested in

Three-dimensional spatial multi-point uniform light focusing through scattering media based on feedback wavefront shaping

Fan Yang(杨帆), Yang Zhao(赵杨), Chengchao Xiang(向成超), Qi Feng(冯祺), and Yingchun Ding(丁迎春)
Chin. Phys. B, 2021, 30 (**4**): 044207. DOI: 10.1088/1674-1056/abe3e6

A scanning distortion correction method based on *X*- *Y* galvanometer Lidar system

Bao-Ling Qi(漆保凌), Chun-Hui Wang(王春晖)†, Dong-Bing Guo(郭东兵), and Bin Zhang(张斌)
Chin. Phys. B, 2021, 30 (**4**): 044206. DOI: 10.1088/1674-1056/abcf42

Optical design of common-aperture multispectral and polarization optical imaging system with wide field of view

Xin Liu(刘鑫), Jun Chang(常军), Shuai Feng(冯帅), Yu Mu(穆郁), Xia Wang(王霞), Zhao-Peng Xu(徐兆鹏)
Chin. Phys. B, 2019, 28 (**8**): 084201. DOI: 10.1088/1674-1056/28/8/084201

Active hyperspectral imaging with a supercontinuum laser source in the dark

Zhongyuan Guo(郭中源), Yu Liu(刘煜), Xin Zheng(郑鑫), Ke Yin(殷科)
Chin. Phys. B, 2019, 28 (**3**): 034206. DOI: 10.1088/1674-1056/28/3/034206

Experimental determination of distributions of soot particle diameter and number density by emission and scattering techniques

Huawei Liu(柳华蔚), Shu Zheng(郑树)
Chin. Phys. B, 2019, 28 (**1**): 014206. DOI: 10.1088/1674-1056/28/1/014206

Incoherent digital holographic spectral imaging with high accuracy of image pixel registration*

Feng-Ying Ma(马凤英)[1], Xi Wang(王茜)[1], Yuan-Zhuang Bu(卜远壮)[1], Yong-Zhi Tian(田勇志)[1], Yanli Du(杜艳丽)[1], Qiao-Xia Gong(弓巧侠)[1], Ceyun Zhuang(庄策云)[2], Jinhai Li(李金海)[1], and Lei Li(李磊)[1,†]

[1] *School of Physics and Microelectronics, Key Laboratory of Materials Physics of the Ministry of Education, Zhengzhou University, Zhengzhou* 450001, *China*

[2] *School of Mechanical Engineering, Zhengzhou University, Zhengzhou* 450001, *China*

(Received 1 October 2020; revised manuscript received 28 November 2020; accepted manuscript online 11 December 2020)

Fresnel incoherent correlation holography (FINCH) is a unique three-dimensional (3D) imaging technique which has the advantages of scanning-free, high resolution, and easy matching with existing mature optical systems. In this article, an incoherent digital holographic spectral imaging method with high accuracy of spectral reconstruction based on liquid crystal tunable filter (LCTF) and FINCH is proposed. Using the programmable characteristics of spatial light modulator (SLM), a series of phase masks, none of whose focal lengths changes with wavelength, is designed and made. For each wavelength of LCTF output, SLM calls three phase masks with different phase constants at the corresponding wavelength, and CCD records three holograms. The spectral images obtained by this method have a constant magnification, which can achieve pixel-level image registration, restrain image registration errors, and improve spectral reconstruction accuracy. The results show that this method can not only obtain the 3D spatial information and spectral information of the object simultaneously, but also have high accuracy of spectral reconstruction and excellent color reproducibility.

Keywords: incoherent digital holography, high-precision registration, spectral imaging, microspectral imaging

PACS: 42.30.–d, 42.40.Ht, 87.64.k–, 87.64.–t **DOI:** 10.1088/1674-1056/abd2aa

1. Introduction

Holography can produce truly three-dimensional images, and be viewed from multiple angles.[1,2] With the rapid development of computer technology and high-resolution image sensor, digital holography exhibit some advantages of high speed, real time, full field of view, and quantitative phase contrast imaging.[3,4] Limited by the requirements for high coherence light source and the unavoidable laser speckle noise, the reconstructed image of digital hologram is seriously ruined by the noise.[5–7] Incoherent digital holography is free from the dependence of traditional digital holography on coherent light sources, and expands its applications to fluorescence microscopy,[8] color holography,[9–14] and adaptive optics.[15,16] By now, many kinds of incoherent digital holography technologies, such as optical scanning holography,[17,18] triangular holography,[19,20] Michelson interferometer type holography,[21,22] and Mach–Zehnder interferometer-type holography[23] have been intensively investigated. Fresnel incoherent correlation holography (FINCH)[24] was first proposed by Joseph Rosen and Gary Brooker in 2007. In the FINCH system, a spatial light modulator (SLM) and a CCD are coaxially arranged to form an in-line incoherent interferometer. It has the advantages of neither time scanning nor space scanning, high resolution, and easy matching with existing mature optical systems.

Spectral imaging technology, which is known as a revolution in the development history of optical instruments, is a perfect combination of spectral technology and imaging technology. The main application field of spectral imaging is remote sensing detection.[25,26] In recent years, its application in microscopy has gradually become a research hotspot. However, there are two common problems in the existing spectral imaging technology: chromatic difference in magnification of spectral images caused by dispersion effect and incapability of extracting 3D information of the target. Chromatic difference in magnification leads to pixel registration errors in spectral images, and thus reducing spectral reconstruction accuracy.[27,28] Spectral imaging can only provide two-dimensional (2D) spatial information of targets in different wavebands, which cannot fully describe the overall characteristics of targets, resulting in low accuracy of 3D recognition. Since the recording and reconstruction of holograms are no longer dependent on coherent light sources, it is possible to combine incoherent digital holography and spectral imaging.

Meanwhile, extending spectral imaging to biomedical

*Project supported by the National Natural Science Foundation of China (Grant Nos. 61505178, 61307019, and 11504333) and the Natural Science Foundation of Henan Province, China (Grant Nos. 18A140032, 15A140038, and 16A140035).

†Corresponding author. E-mail: lilei@zzu.edu.cn

© 2021 Chinese Physical Society and IOP Publishing Ltd

engineering has unparalleled great potential for researchers to obtain more information about organs, tissues, and even cells.[29,30] One of the commonly used optical methods is the spectral diagnostic technique, which can obtain the entire spectrum of a single tissue site within a specific wavelength region. This method is often referred to as the point measure method, but it cannot provide spatial information of samples. According to the dispersion theory of light, the focusing region will move accordingly with wavelength increasing. When the object distance is less than the recording distance, it will cause some single-band images to become blurred with the increase of wavelength. This problem may not be ignored in the application of microspectral imaging.

In this work, an incoherent digital holographic spectral imaging system based on liquid crystal tunable filter (LCTF) and SLM is built. A serious of double-lens phase masks, none of whose focal lengths changes with wavelength, is designed and made. For each wavelength of LCTF output, SLM calls the phase masks of the corresponding wavelength, and CCD records the spectral holograms. The spectral images obtained by this method have a constant magnification, which can achieve pixel-level image registration, restrain image registration errors, and improve spectral reconstruction accuracy. Moreover, by replacing specific phase mask loaded on the SLM, we avoid the technical conundrum caused by dispersion theory. The incoherent digital spectral holographic system based on LCTF not only improves the capability of microscopic imaging, but also records and extracts the phase information, amplitude information, and color information of the stained cells.

2. Principle of holographic spectral imaging

Figure 1 shows the schematic of the incoherent digital holographic spectral imaging system. A broadband light source passes through an LCTF and provides a continuous tunable narrowband incoherent illumination with a full width at half maximum (FWHM) value of 10 nm. An ideal point source located at $(x_s, y_s, -z_s)$, a distance z_s from a spherical positive lens with f_0 focal length, induces a diverging spherical wave on the lens plane in the form of $C(\overline{r_s})L(-\overline{r_s}/z_s)Q(1/z_s)$, where $C(\overline{r_s}) = \exp[\mathrm{i}\pi(z_s\lambda)^{-1}(x_s^2+y_s^2)]$ is a complex constant dependent on the location of the point source, $L(\overline{r_s}) = \exp[\mathrm{i}2\pi\lambda^{-1}(x_s x+y_s y)]$ and $Q(b) = \exp[\mathrm{i}\pi b\lambda^{-1}(x^2+y^2)]$ denote the linear phase function and the quadratic phase function, respectively. Passing through the lens, and propagating additional distance of d till the SLM plane, the complex amplitude becomes $C(\overline{r_s})L(-\overline{r_s}/z_s)Q(1/z_s)Q(-1/f_0)*Q(1/d)$.

The SLM is space-division multiplexed by two diffractive lenses with focal lengths of f_{d1} and f_{d2}. Because of the diffraction effect, the effective focal length of the lens producing chromatic aberration is inversely proportional to the wavelength as shown in the formula $f = r^2/N\lambda$. Here r is the radius of diffraction lens and N is the Fresnel number. When λ_0 is the working wavelength of the mask and the imaging wavelength is λ, the effective focal lengths of the two lenses are $\lambda_0 f_{d1}/\lambda$ and $\lambda_0 f_{d2}/\lambda$, respectively. Therefore, the reflection function of SLM is expressed as

$$R(x,y) = B\exp\left[-\frac{\mathrm{i}\pi}{\lambda(\lambda_0 f_{d1}/\lambda)}(x^2+y^2)\right] + B'\exp\left[-\frac{\mathrm{i}\pi}{\lambda(\lambda_0 f_{d1}/\lambda)}(x^2+y^2)+\mathrm{i}\theta_j\right]. \quad (1)$$

Here B and B' are constants, θ_j $(j = 1, 2, 3)$ are constant phase shifts, which are used to eliminate the conjugate and zero-order images. After the two beams travel a distance of z_h, the interference pattern occurring on the CCD surface is the point spread function (PSF) of the system and can be expressed as

$$\begin{aligned} &I_p(x,y,\overline{r_s},z_s,\lambda) \\ &= \left|C(\overline{r_s})L\left(\frac{-\overline{r_s}}{z_s}\right)Q\left(\frac{1}{z_s}\right)Q\left(-\frac{1}{f_0}\right)*Q\left(\frac{1}{d}\right)\right. \\ &\quad \left.\times R(x,y)*Q\left(\frac{1}{z_h}\right)\right|^2 \\ &= C + C_1\exp\left\{\frac{\mathrm{i}\pi}{\lambda z_r(\lambda)}\left[(x-M_T x_s)^2\right.\right. \\ &\quad \left.\left.+(y-M_T y_s)^2\right]+\mathrm{i}\theta\right\}+\mathrm{c.c.}, \end{aligned} \quad (2)$$

where

$$z_r(\lambda) = \frac{[f_1(\lambda)+z_h(\lambda)][f_2(\lambda)+z_h(\lambda)]}{[f_2(\lambda)-f_1(\lambda)]}$$

is the reconstructed distance, with

$$f_{1,2}(\lambda) = \frac{\lambda_0 f_{d1,2}(f_e+d)}{\lambda_0 f_{d1,2}-\lambda(f_e+d)}, \quad f_e = \frac{z_s f_0}{f_0-z_s},$$

M_T is the lateral magnification, c.c. is the complex conjugate of the second term on the right.

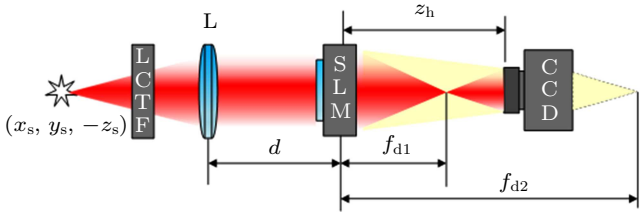


Fig. 1. Schematic diagram of incoherent digital spectral holography. LCTF: liquid crystal tunable filter; L: collimating lens; SLM: spatial light modulator; CCD: charge-coupled device.

In order to satisfy the optimum interference condition of two beams after being split by SLM, the distance z_h between CCD and SLM needs to be adjusted continuously with the imaging wavelength. In other words, when the two cones of the spherical waves are perfectly overlapped with each other, the optimal contrast between interference fringes can be

achieved. The z_h can be obtained from the triangular similarity relationship in Fig. 1 as follows:[31]

$$z_h(\lambda) = \frac{2\lambda_0 f_{d1} f_{d2}}{\lambda(f_{d1}+f_{d2})}. \tag{3}$$

The incoherent hologram of a general 3D object $g(x_s, y_s, z_s)$ is

$$H(x,y) = \iiint g(x_s,y_s,z_s) I_p(x,y,\overline{r_s},z_s,\lambda)\,\mathrm{d}x_s\,\mathrm{d}y_s\,\mathrm{d}z_s. \tag{4}$$

That is to say, in order to accurately adjust the value of z_h, the mechanical scanning device needs to be introduced into the system, which will bring some errors inevitably, and change the transverse magnification of the system as shown in the following formula:

$$M_T(\lambda) = -\frac{z_h(\lambda) f_0}{z_s f_0 + d(f_0 - z_s)}. \tag{5}$$

The change of transverse magnification of spectral image will lead to image registration errors, resulting in the inaccurate extraction of relative spectral intensity.

In order to obtain 3D images with high spectral reconstruction accuracy, a high-precision spectral imaging technology and method based on FINCH is proposed. A series of dual lens phase masks with constant focal lengths of f_{d1} and f_{d2} at different wavelengths is designed and made. Using the programmable characteristics of SLM, for each wavelength of LCTF output, SLM calls the masks of the corresponding wavelength. Three holograms with different phase constants are recorded sequentially by CCD. Using three-step phase shift technology, three holograms are linearly superimposed to eliminate the zero-order and twin image, thus obtaining the complex value hologram $H_F(x,y)$,

$$\begin{aligned} H_F(x,y) &= H_1(x,y)[\exp(\mathrm{i}\theta_3) - \exp(\mathrm{i}\theta_2)] \\ &\quad + H_2(x,y)[\exp(\mathrm{i}\theta_1) - \exp(\mathrm{i}\theta_3)] \\ &\quad + H_3(x,y)[\exp(\mathrm{i}\theta_2) - \exp(\mathrm{i}\theta_1)] \\ &= \iiint g(x_s,y_s,z_s)\exp\left\{-\frac{\mathrm{i}\pi}{\lambda z_r(\lambda)}[(x - M_T x_s)^2 \right. \\ &\quad \left. + (y - M_T y_s)^2]\right\}\mathrm{d}x_s\,\mathrm{d}y_s\,\mathrm{d}z_s. \end{aligned} \tag{6}$$

The reconstructed image is obtained by simulating Fresnel diffraction process on the computer, and then the 3D spectral image $S(x', y', z_r)$ can be reconstructed from complex-valued holograms as follows:

$$\begin{aligned} &S(x',y',z_r) \\ &= \iint H_F(x,y)\exp\left\{\frac{\mathrm{i}\pi}{\lambda z_r(\lambda)}[(x'-x)^2 + (y'-y)^2]\right\}\mathrm{d}x\mathrm{d}y. \end{aligned} \tag{7}$$

Using this method to record the spectral holograms, we can realize that the recorded distance, spectral holograms, reconstruction distance, and spectral reconstruction images are independent of wavelength, and the reconstructed images have the same lateral magnification, which can avoid the mechanical error caused by space scanning and suppress the registration error in spectral image fusion.

Suppose that the spectral power distribution of the incoherent light source is $I(\lambda)$, the spectral transmittance of the LCTF is $T(\lambda)$, the spectral reflectance function of the object surface is $R_{i,j}(\lambda)$, the spectral sensitivity function of CCD is $S(\lambda)$, the spectral power distribution of each pixel in the reconstructed image is $I_{i,j}(\lambda)$, the exposure coefficient of the camera remains unchanged during the recording of spectral holograms, then the reconstructed image will be obtained by using angular spectrum diffraction algorithm, so the pixel size of the reconstructed image is equal to that of CCD, the reflectance of reconstructed image can be expressed as follows:

$$R_{i,j}(\lambda) = \frac{I_{i,j}(\lambda)}{\int I(\lambda)T(\lambda)S(\lambda)\,\mathrm{d}\lambda}. \tag{8}$$

The spectral response function of optical instrument is obtained from the instruction manual provided by the instrument manufacturer. Formula (8) is used to extract and calculate the spectral power distribution of pixels in the reconstructed image.

3. Experimental results

In this section, we take the dice, trinkets and biological samples as experimental objects, confirm the feasibility of this method, and realize the high precision microscopic spectral imaging of cells.

3.1. Spectral imaging optical path design based on FINCH

The schematic of the spectral imaging system based on FINCH is shown in Fig. 2.

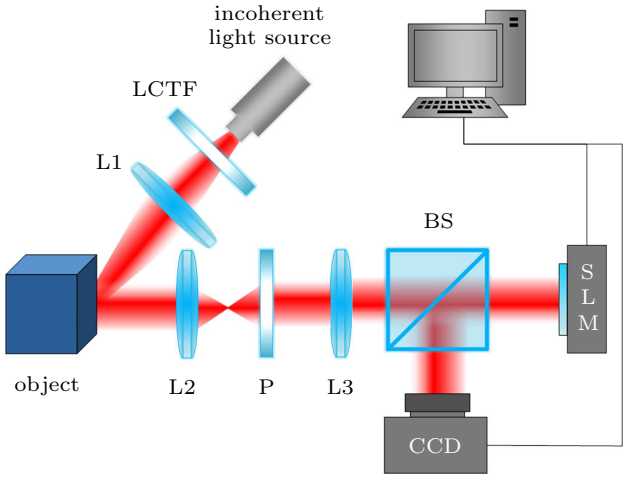


Fig. 2. Schematic diagram of spectral imaging system based on LCTF and FINCH. Incoherent light source, xenon lamp; L1, L2, L3: converging lens; P: polarizer; BS: beam splitters.

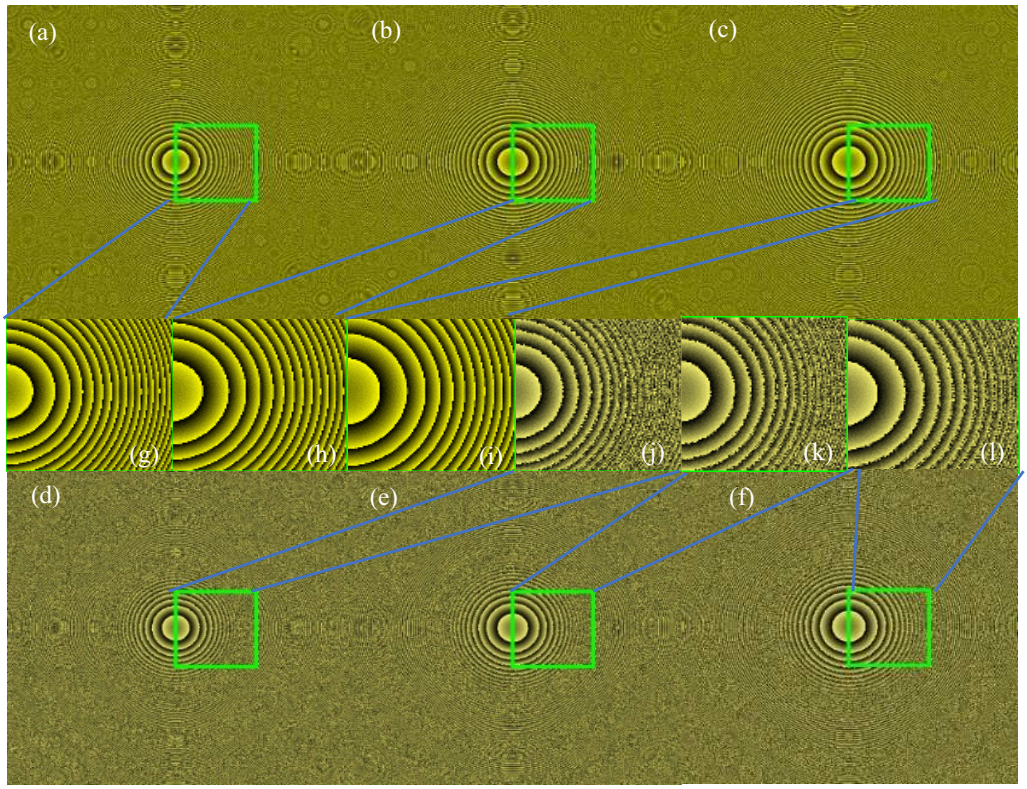


Fig. 3. Single [(a)–(c) focal length of 255 mm] and dual [(d)–(f), focal lengths of 245 mm and 255 mm, random pixel mixing] lens phase masks with 0 phase shift at selected wavelengths of [(a), (d)] 450 nm, [(b), (c)] 550 nm, and [(e), (f)] 650 nm; (g)–(i) and (j)–(l), enlargement of parts in green rectangular boxes shown in panels (a)–(c) and (d)–(f), respectively.

Spatially incoherent illumination with controllable wavelength required for the test, which is generated by an incoherent xenon lamp source (CEL-TCX250, 250 W) and LCTF (VariSpec Liquid Crystal Tunable Filters, 400 nm–720 nm, FWHM 10 nm). The focal lengths of L1, L2, and L3 are 60 mm, 60 mm, and 250 mm, respectively. For the convenience of subsequent processing, only pixels in CCD (Q-IMAGING digital camera RETIGA 6000, pixel size $\sigma_c = 4.54$ μm, pixel array) are used. The SLM is a series of phase masks only, (Holoeye Pluto, 1920×1080 pixels, 8-μm pixel pitch). The polarization direction of the polarizer is the same as that of the SLM. The other specifications of the experiment are as follows: $f_{d1} = 245$ mm, $f_{d2} = 255$ mm, $z_h = 250$ mm, $d = 150$ mm (which is the distance from L3 to the SLM).

Single and dual lens phase masks with 0 phase shift at selected wavelengths are shown in Fig. 3. Figures 3(a)–3(c) show single lens phase masks with the same focal length of 255 mm at 450 nm, 550 nm, and 650 nm, respectively. As can be seen, when the focal length and aperture of the diffraction lens are kept unchanged, the concentric rings of the phase mask become more and more sparse with the increase of the wavelength. The same trend is shown in Figs. 3(d)–3(f), in which the dual lens masks using a random pixel mixing space division multiplexing have a focal length of 245 mm and 255 mm at 450 nm, 550 nm, and 650 nm, respectively.

3.2. Imaging results

The spectral holograms of two white dices with black dots are recorded from 400 nm to 700 nm in intervals of 10 nm. Figures 4(a)–4(o) show the selected spectral images from 560 nm to 700 nm in intervals of 10 nm. Figure 4(p) shows the spectrum of the point on the dice shown in the inset, and the corresponding CIE1931 chromaticity coordinates ($x = 0.3552$, $y = 0.3448$) are shown in Fig. 4(q). For comparison, a cell phone camera picture of the two dices is shown in the inset of Fig. 4(q). It can be seen that the incoherent holographic spectral imaging system can accurately reconstruct the color information of the object.

Figure 5 shows color imaging results of a Poker ear stud at wavelengths of 672.8 nm, 562.8 nm, and 452.8 nm. Figures 5(a)–5(c) show the reconstructed images at 672.8 nm, 562.8 nm, and 452.8 nm. The color composite image is shown in Fig. 5(d). For comparison, a cell phone camera picture and the color spectral image obtained from commercial imaging spectrometer Hyperspec VNIR (400 nm–900 nm) are shown in Figs. 5(e) and 5(f). The structural similarity index is 0.68524 measured by this method, and 0.66336 by the commercial spectrometer. The results show that the color reproducibility of the reconstructed image obtained by this method is better than that by the commercial imaging spectrometer.

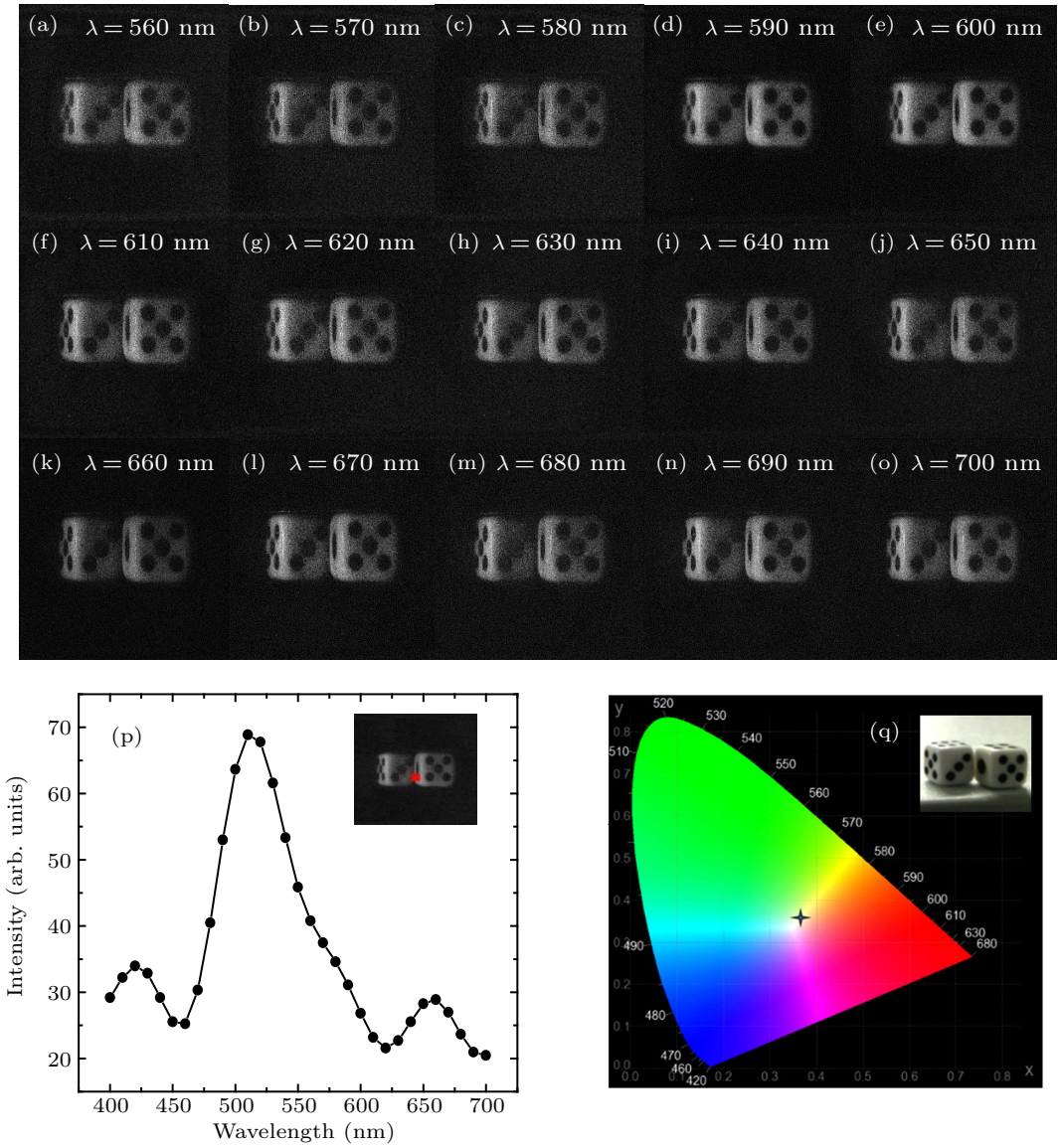


Fig. 4. Spectral imaging results of dice: (a)–(o) selected spectral images from 560 nm to 700 nm in intervals of 10 nm, (p) spectrum of point on dice shown in inset, (q) CIE1931 chromaticity coordinates of point, with inset showing cell phone camera picture of two dices.

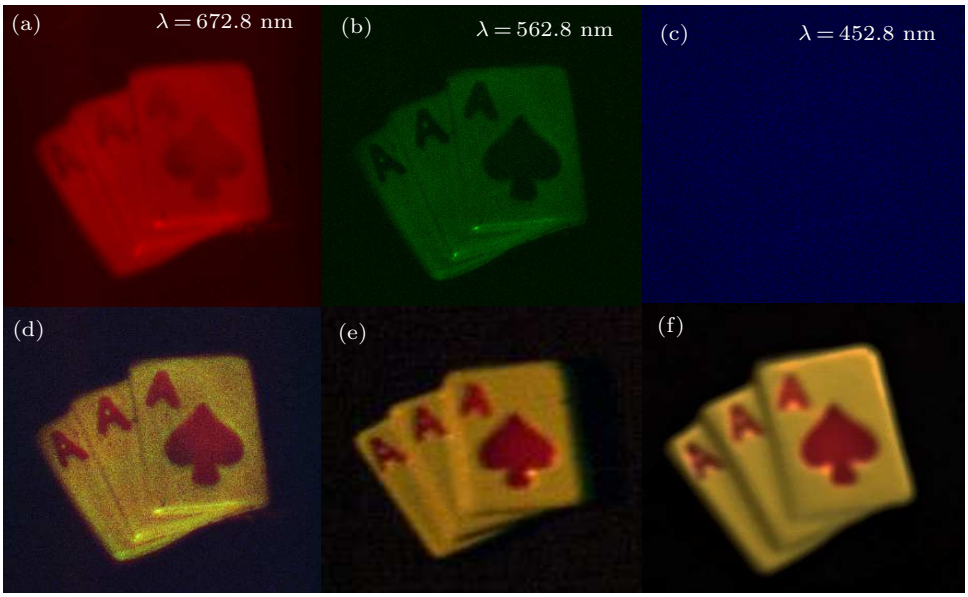


Fig. 5. Color imaging results of the Poker ear stud: (a)–(c) reconstructed images at wavelengths of 672.8 nm, 562.8 nm, and 452.8 nm; (d) color composite image from panels (a)–(c); (e) cell phone camera picture; (f) imaging result from commercial imaging spectrometer.

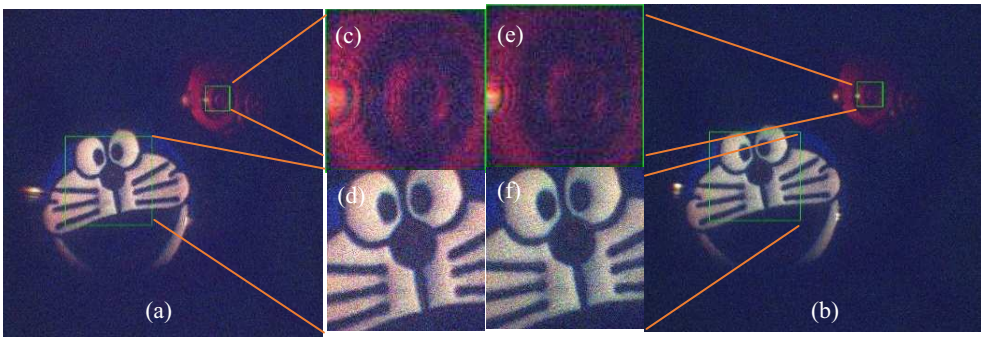


Fig. 6. Composited color images of ear suds at different reconstruction distances: ((a), (b)) reconstructed images in the best focal plane of red mask and Doraemon, respectively; (c), (d) and (e), (f) magnified parts in green rectangular boxes shown in panels (a) and (b), respectively.

Using the same method, we study the color three-dimensional spectral imaging characteristics of the system. The tested objects are two ear studs with 2 cm apart. The spectral holograms are recorded from 400 nm to 700 nm, in an interval of 20 nm. The composited color images are shown in Fig. 6. Figures 6(a) and 6(b) show the composited color reconstructed images in the best focal plane of the red mask and Doraemon, respectively. Figures 6(c)–6(f) are the magnified parts in rectangular boxes shown in Figs. 6(a) and 6(b). The results show that the FINCH system 3D spectral image with high accuracy of image pixel registration can be achieved by keeping the transverse magnification constant in the spectral imaging process.

3.3. Incoherent digital holographic microspectral imaging based on LCTF

Amicroscopic imaging system based on FINCH is built, a 20×, 0.4-NA microscope objective with a working distance of 5.9 mm is placed in front of the polarizer. Figures 7(a)–7(c) show the holograms of the stem transected cells of stained woody dicotyledons with phase factors of 0°, 120°, and 240° at 632.8 nm. The complex amplitude and phase diagram are shown in Figs. 7(d) and 7(e), respectively. Figure 7(f) shows the spectrum of the green point on the cells indicated in the inset.

Figures 8(a) and 8(c) show the microscopic imaging results from FINCH microscope and Nikon microscope, respectively. Figure 8(b) shows the enlargement in the green box in Fig. 8(a). The green dots in Figs. 8(b) and 8(c) represent the same cell. Although the performance of the spectral microscopy system based on incoherent digital holography needs to be further optimized, compared with commercial optical microscope, it has significant advantages in obtaining 3D spatial information and spectral information of biological samples.

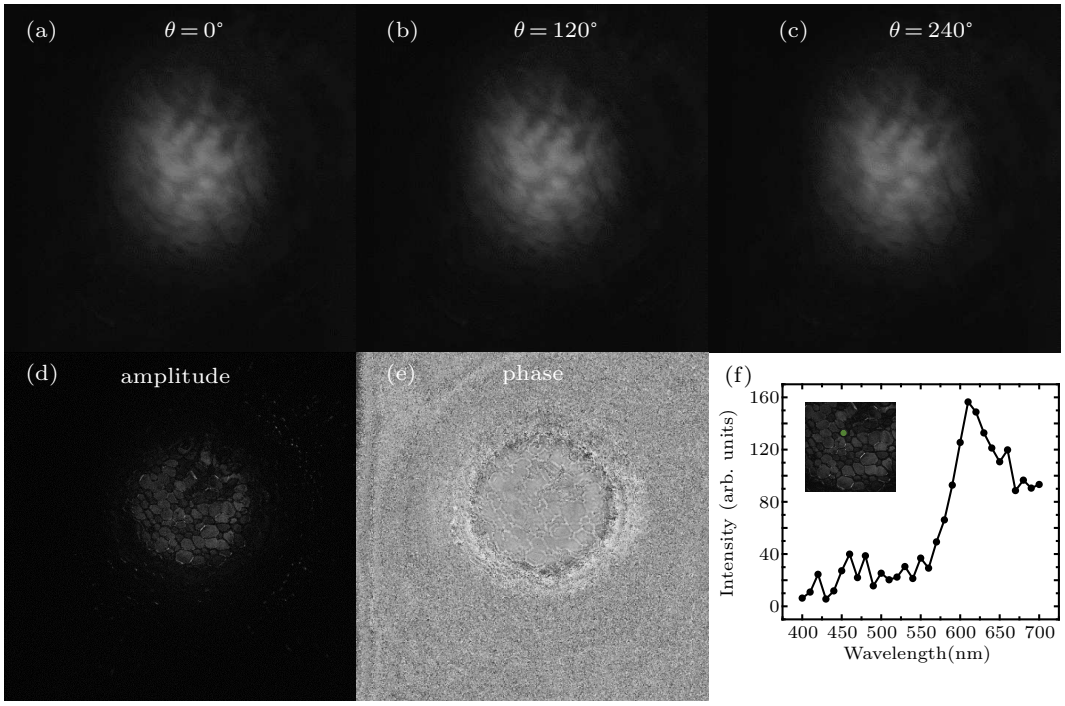


Fig. 7. (a)–(c) Holograms at 632.8 nm with 0°, 120°, and 240° phase factors; (d), (e) amplitude and phase of complex hologram; (f) spectrum of green point on cells shown in inset.

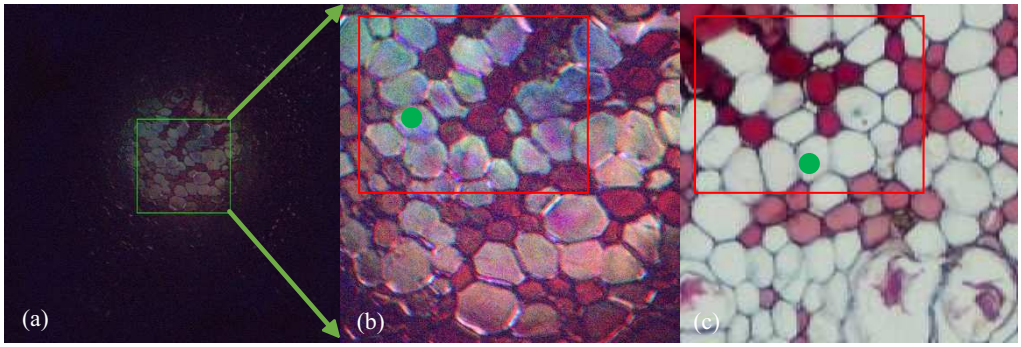


Fig. 8. (a) Spectral fusion image of stem transversely cut cells stained with woody dicotyledonous plant; (b) enlargement of green box in panel (a); (c) image from NIKON microscope.

4. Conclusions and perspectives

In this paper, a high-precision spectral imaging technology and method based on FINCH is proposed and analyzed theoretically in detail. By designing the phase masks loaded on SLM, the system has a constant transverse magnification at different imaging wavelengths, which avoids the mechanical error caused by space scanning and suppresses the registration error in spectral image fusion. The results show that this method can not only obtains the 3D spatial information and spectral information of the object simultaneously, but also has high accuracy of spectral reconstruction and excellent color reproducibility. This method has the potential applications in imaging and detection in label-free biological samples.

Acknowledgment

The authors would like to thank the following collaborators: Ms. Wang X, Mr. Bu Y Z, Prof. Li L, Prof. Tian Y Z, Prof. Du Y L, Prof. Gong Q X, Mr. Zhuang C Y, Mr. Li J H, for their contributions to the present work.

References

[1] Zhang Q S, Lu X X, Yu Q T and Liu G Y 2009 *Chin. Phys. B* **18** 2764
[2] Wang F, Xiao W, Pan F, Liu S, Cong L, Li R, Rong L and He A 2011 *Opt. Laser Eng.* **49** 903
[3] BjornK, Andreas B, Angelika V, Steffi K, Patrik L, Johannes M, Helge K and Gert V B 2010 *J. Biomed. Opt.* **15** 036009
[4] Marquet P, Rappaz B, Magistretti P J, Cuche E, Emery Y, Colomb T and Depeursinge C 2005 *Opt. Lett.* **30** 468
[5] Cai L Z, Meng X F, Meng X F, Wang Y R, Shen X X, Dong G Y and Yang X L 2006 *Opt. Commun.* **259** 64
[6] Hong J and Kim M K 2013 *J. Eur. Opt. Soc. Rapid. Publ.* **8** 13077
[7] Man T, Wan Y, Wu F and Wang D Y 2015 *Opt. Commun.* **355** 109
[8] Rosen J, Siegel N and Brooker G 2011 *Opt. Express* **19** 26249
[9] RosenJ and Brooker G 2007 *Opt. Express* **15** 2244
[10] Kim and Myung K 2013 *Opt. Express* **21** 9636
[11] Tomasz K and Maksymilian C 2016 *Opt. Express* **24** 2189
[12] Hara T, Tahara T, Ichihashi Y, Oi R and Ito T 2020 *Opt. Express* **28** 10078
[13] Yaraş F, Kang H and Onural L 2009 *Appl. Opt.* **48** H48
[14] Endo Y, Tahara T and Okamoto R 2019 *Appl. Opt.* **58** G149
[15] Kim M K 2012 *Opt. Lett.* **37** 2694
[16] Kim M K 2013 *Appl. Opt.* **52** A117
[17] Liu J P 2015 *Appl. Opt.* **54** A59
[18] Rivenson Y, Stern A and Rosen J 2011 *Opt. Express* **19** 6109
[19] Naik D N, Pedrini G and Osten W 2013 *Opt. Express* **21** 3990
[20] Wan Y H, Man T L and Wang D Y 2014 *Opt. Express* **22** 8565
[21] Choi K, Hong K, Park J and Min S W 2020 *Appl. Opt.* **59** 1948
[22] He J R, Ren H, Xu T X, Gong Q X, Du Y L, Liu X M, Shan C X, Su J P and Ma F Y 2019 *J. Opt.* **21** 025701
[23] Pedrini G, Li H, Faridian A and Osten W 2012 *Opt. Lett.* **37** 713
[24] Rosen J and Brooker G 2007 *Opt. Lett.* **32** 912
[25] Lee Z P, Shang S L, Hu C M and Zibordi G 2014 *Appl. Opt.* **53** 3301
[26] Yang J F, Wan J H, Ma Y, Zhang J, Hu Y B and Jiang Z C 2019 *J. Coastal Res.* **90** 332
[27] Wang D N, Grattan K T V and Palmer A W 1996 *Opt. Commun.* **127** 19
[28] Cui J H, Zhang S S, Jiang Z Y, Liu P and Li L 2020 *J. Appl. Remote Sens.* **14** 026520
[29] Luo Y, Loannis K Z, Oh S B, Kamm R D and Barbastathis G 2011 *J. Biomed. Opt.* **16** 096015
[30] Carver G E, Locknar S A, Morrison W A, Ramanujan Krishnan V and Farkas D L 2014 *J. Biomed. Opt.* **19** 036016
[31] Katz B, Rosen J, Kelner R and Brooker G 2012 *Opt. Express* **20** 9109